Combining Membrane Potential Imaging with Other Optical Techniques

Nadia Jaafari, Kaspar E. Vogt, Peter Saggau, Loew M Leslie, Dejan Zecevic, Marco Canepari

Chapter 4: Combining Membrane Potential Imaging With Other Optical Techniques

Nadia Jaafari[1,2,3], Kaspar E Vogt[4], Peter Saggau[5], Loew M Leslie, Dejan Zecevic[7], Marco Canepari[1,2,3]

1 Inserm U836, Grenoble Institute of Neuroscience, Team 3, Grenoble Cedex 09, France

[2] Université Joseph Fourier, Laboratoire Interdisciplinare de Physique (CNRS UMR 5588), France

[3] Laboratories of Excellence, Ion Channel Science and Therapeutics, France

[4] International Institute for Integrative Sleep Medicine, University of Tsukuba, Tsukuba Ibaraki, Japan

[5]Department of Neuroscience, Baylor College of Medicine, Houston, TX 77030

[6] Center for Cell Analysis and Modeling, University of Connecticut Health Center, Farmington, Connecticut, USA

[7] Department of Cellular and Molecular Physiology, Yale University School of Medicine, New Haven, CT 06520, USA

Corresponding author: Marco Canepari, Laboratoire Interdisciplinaire de Physique (LIPhy), Université J. Fourier et CNRS UMR 5588, Bat. E45, 140 avenue de la physique, Domaine univ., 38400 St Martin d'Hères, B.P. 87 38402 St Martin d'Hères cedex, France.

Tel. +33 (0)4 76 51 47 31

Email: marco.canepari@ujf-grenoble.fr

Abstract

Membrane potential imaging using voltage-sensitive dyes can be combined with other optical techniques for a variety of applications. Combining voltage imaging with Ca^{2+} imaging allows correlating membrane potential changes with intracellular Ca^{2+} signals or with Ca^{2+} currents. Combining voltage imaging with uncaging techniques allows analyzing electrical signals elicited by photorelease of a particular molecule. This approach is also a useful tool to calibrate the change in fluorescence intensity in terms of membrane potential changes from different sites permitting spatial mapping of electrical activity. Finally, combining voltage imaging with optogenetics, in particular with channelrhodopsin stimulation, opens the gate to novel investigations of brain circuitries by allowing measurements of synaptic signals mediated by specific sets of neurons. Here we describe in detail the methods of membrane potential imaging in combination with other optical techniques and discus some important applications.

1 Introduction

The advantages of the optical measurements of membrane potential (V_m), over electrode recordings, are the possibility to record voltage changes at high spatial resolution and from a very large number of sites and the ability to probe structures too small to tolerate electrodes. Combining this measurement with another optical measurement or with an optical stimulation at the same spatial resolution and scale allows investigating and understanding the voltage-dependence of a variety of physiological phenomena or the changes of V_m produced by activation of a particular signaling pathway as well as by a well-defined stimulation protocol. In this chapter we describe in detail the main optical techniques that have been so far successfully combined with V_m imaging: calcium (Ca^{2+}) imaging, photorelease of caged compounds and optogenetic photostimulation. At the end of this chapter we discuss the case of V_m imaging combined with channelrhodopsin (ChR) stimulation, which is becoming a fundamental experimental approach in neurophysiology.

Combined optical measurements have been widely used in biology for a long time. In molecular biology, for instance, the concomitant localization of two or more proteins is achieved by using fluorescent antibodies with different absorption and emission spectra. Combined imaging of two different physiological parameters requiring sequences of signal acquisitions was more difficult to achieve until twenty years ago. Thus, before the introduction of more sophisticated imaging systems, combined optical recordings at relatively slow rate and using two indicators have been utilized to measure intracellular pH and Ca^{2+} (Martinez-Zaguilan et al. 1991) as well as slow V_m changes and Ca^{2+} signals (Kremer et al. 1992). Combined functional imaging is therefore an experimental approach that evolved in the last two decades in parallel with advancements in imaging technology. The correlation of a V_m recording with a measurement of a Ca^{2+} signal is perhaps the most important case of dual optical measurement of a functional signal (Canepari et al. 2008). Indeed, crucial information on Ca^{2+} influx from the extracellular space comes from the fact that Ca^{2+} signals are directly correlated with V_m when they originate from Ca^{2+} channels in the plasma membrane. This category includes voltage-gated Ca^{2+} channels (VGCCs), glutamate receptors (in particular NMDA receptors) and other Ca^{2+} permeable pores. In all these cases, the charge influx associated with Ca^{2+} contributes, to a different extent, to the current underlying depolarization. In addition, the biophysical properties of several Ca^{2+} signals in the plasma membrane also depend on membrane depolarization. For instance, Ca^{2+} influx via VGCCs is voltage-dependent since depolarization is necessary for channel opening. Similarly, Ca^{2+} influx via NMDA receptors is voltage-dependent since depolarization is necessary to unblock the channel from Mg^{2+}. In contrast, Ca^{2+} signals are not directly correlated with V_m when they are due to Ca^{2+} flux through

internal membranes. For example Ca^{2+} release from internal store is not directly correlated with V_m. In this case, Ca^{2+} flux does not contribute to the current underlying the V_m change.

Among photostimulations combined to V_m imaging, chemical stimulation delivered by photorelease of a molecule from a caged compound is a powerful tool to explore many physiological phenomena. Notably, uncaging of principal neurotransmitter such as glutamate or GABA, allows investigating how local activation of synaptic receptors produces or modulates V_m in different sub-cellular sites (Vogt et al. 2011b). V_m imaging can be also combined with ChR stimulation expressed in sub-sets of well identified neurons. This application may provide new information on the function of local neuronal circuits (Tsuda et al. 2013).

The techniques of V_m imaging described in this chapter are achieved by recording signals from organic voltage-sensitive dyes. Unless specified otherwise, this type of signal is expressed as a fractional change in fluorescence intensity $\Delta F/F_0 = (F(t) - F(t_0))/F(t_0)$, where F(t) is the recorded fluorescence intensity at a given time and $F(t_0)$ is the fluorescence intensity at the resting membrane potential (resting fluorescence). Finally, most of the examples in this chapter are recordings from individually-stained single-neurons described in the previous chapter.

2 Principles of combining two optical techniques

The combination of two optical techniques is typically achieved by using two photosensitive molecules. These molecules can be indicators, for instance fluorescence dyes, or molecules that produce a stimulation of the cell upon light activation. If one of the two molecules is used for photostimulation, for instance a caged compound or a photo-sensitive protein, achieving simultaneous imaging requires that this molecule is not excited by the same wavelength used for excitation of the imaging indicator. This requirement is straightforward to achieve for many caged compounds that are activated exclusively by UV light and that can be combined with indicators excited in the visible range. In contrast, combining imaging techniques with ChR stimulation is more difficult since ChR is activated by light over a broad visible spectrum. If the two molecules are both fluorescent indicators, for instance a voltage-sensitive dye and a Ca^{2+} indicator, combined imaging can be achieved in three different ways depending on the optical properties of the two indicators. First, the two indicators may have separate absorption spectra but a largely overlapping region in the emission spectra. Second, the two indicators may have a large overlapping region in their absorption spectra but well separated emission spectra. Third, the two indicators may have a separation both in the absorption and in the emission spectra.

Fig. 4.1 shows three examples of spectral representations for the different cases and the optical arrangements to combine the recording of the two signals. In the first case (Fig. 4.1a), the fluorescence from the two dyes can be excited using two separate wavelengths and the emitted light from the two indicators is recorded using a single detector. In this case, it is never possible to achieve a simultaneous measurement since the imaging experiment requires alternating between the two different excitation wavelengths. In the second case (Fig. 4.1b), because the excitation spectra are overlapping, fluorescence from both indicators can be excited using the same excitation wavelength. Emitted light can be recorded by two different detectors after splitting the emitted light with a secondary dichroic mirror. Thus, by synchronizing data acquisition of the two detection systems, it is possible to achieve simultaneous imaging of the fluorescence signals from the two indicators. Finally, in the third case (Fig. 4.1c), the combined excitation and detection of the two fluorescence systems can be done using two excitation wavelengths and two detection systems simultaneously.

The optimization of recording signals from two indicators depends on the availability of probes with narrow excitation and emission bands. This is not the case for the available fast voltage sensitive dyes. Most of the styryl voltage dyes are characterized by a broad excitation spectrum in the visible range and a broad emission spectrum in the red-IR region (Fluhler et al. 1985). Fig. 4.2 shows the absorption and emission spectra of the hydrophobic voltage-sensitive dye di-8-ANEPPS which are similar to those of di-4-ANEPPS and of the water soluble indicators JPW-1114 (di-2-ANEPEQ) and JPW-3028 (di-1-ANEPEQ) all based on the same chromophore. Similar spectral properties are also shared by many of the commonly used “RH” dyes such as RH-795, RH-237, RH-421 and RH-414. With these dyes, well separated spectra are difficult to obtain using commercially available Ca^{2+} indicators excited in the visible spectral range. Nevertheless, the combined recordings are still possible due to a large Stokes shift of charge-shift voltage probes (~150 nm). In addition, more efficient combined recordings can be achieved using Ca^{2+} indicators excited in the UV spectral range.

Both voltage dyes and Ca^{2+} indicators can be loaded into cells either by extracellular bath application of the indicator or by intracellular injection using either a patch-electrode or a sharp microelectrode. For extracellular loading, Ca^{2+} dyes are commercially available in membrane-permeant AM-ester form. Once in the cell, the acetyl-ester is hydrolyzed by the endogenous esterases and the released free indicator remains in the cytoplasm (Yuste, 2000). For intracellular loading, Ca^{2+} indicators are available as water-soluble potassium salts. When injected into cells from a patch electrode, the dye can quickly equilibrate in the cytosol at a given concentration permitting quantitative estimate of Ca^{2+} signals (Eilers and Konnerth, 2000). In general, intracellular loading of the Ca^{2+} indicator is done in conjunction with the intracellular loading of the voltage sensitive dye. It is also possible to load the cell with the voltage sensitive dye first and include the Ca^{2+} indicator in the pipette used for re-patching the

labeled cell. In this protocol, V_m imaging is carried out first, immediately after re-patching, during which time the cell is loaded with the Ca^{2+} indicator from the recording pipette.

3 Combining V_m and Ca^{2+} imaging

3.1 Combining V_m and Ca^{2+} imaging in sequential way

Commonly used voltage sensitive dyes such as di-4-ANEPPS, di-8-ANEPPS and Di-2-ANEPEQ (JPW-1114) have wide excitation spectrum in the blue/green region and wide emission spectrum in the red/IR region (Fig. 4.2). If combined with Fluo, Calcium Green or Oregon Green Ca^{2+} indicators, both dyes can be excited by a blue wavelength (which, however, is not optimal for the voltage-sensitive dye) and green (Ca^{2+}) and red (V_m) fluorescence can be recorded separately. Voltage sensitive dye excitation is optimal at 532 nm (Canepari et al. 2010). Thus, if combined with UV-excitable Fura indicators, the voltage-sensitive dye can be excited at its optimal visible wavelength and, as with the previous combination, the two emission signals can be recorded separately.

Although both types of combinations allow simultaneous measurement of V_m and Ca^{2+} fluorescence, many studies were initially performed through sequential recordings of the two optical signals. Combined V_m and Ca^{2+} imaging from individual neurons using blue-excitable/green-emitting Ca^{2+} indicators has been also used in several other studies. In the barrel cortex, the high-affinity indicator Oregon Green BAPTA-1 was combined with the voltage sensitive dye JPW-1114 in recordings from individual neurons and with the voltage indicator RH-1691 in *in vitro* and *in vivo* network recordings (Berger et al. 2007). In prefrontal cortical neurons, dendritic recordings were obtained combining JPW-1114 either with the high-affinity Ca^{2+} indicator Calcium Green-1 or with the low-affinity Ca^{2+} indicator Fluo-5F (Milojkovic et al. 2007).

The use of UV-excitable Fura indicators minimizes the spectral overlap with the voltage-sensitive dye. Additionally, the voltage-sensitive dye is not excited during Ca^{2+}-imaging preventing a substantial photodynamic damage that can occur during relatively long recording periods (Canepari et al., 2008). UV-excitable Fura indicators with different equilibrium constants (K_d) are commercially available (see Table 4.1). This permits the choice of the most suitable indicator for the measurement of either the Ca^{2+} influx (high-affinity indicator) or the change in intracellular free Ca^{2+} concentration (low-affinity indicator).

Dye	K_d (µM)	K_{dye}(300µM)	K_{dye}(1mM)
fura-2	0.224 [(a)]	~1300	~4500
fura-5F	0.4 [(a)]	~750	~2500

bis-fura-2	0.525 [(a)]	~570	~1900
fura-4F	0.77 [(a)]	~390	~1300
fura-6F	5.3 [(a)]	~57	~190
fura-FF	10 [(b)]	~30	~100
Mag-fura-2	25 [(c)] - 40 [(d)]	~7.5-12	~25-40

Table 4.1: Dissociation constants and buffering capacities of Fura dyes. A list of commercially available Fura dyes with dissociation constant (K_d) and buffering capacities (K_{dye}) at the two concentrations of 300 µM and 1 mM. References: [(a)] Invitrogen - Molecular Probes handbook (for fura-2 and bis-fura-2 at 1 mM Mg^{2+}); [(b)] Schneggenburger et al. 1999; [(c)] Hyrc et al. 2000; [(d)] Naraghi 1997.

In contrast to the indicators excited in the visible range, Fura indicators allow ratiometric measurements. When excited above their isosbestic wavelength (~360 nm), the changes of fluorescence associated with an increase in Ca^{2+} concentration are negative. Imaging above the isosbestic wavelength has several advantages. First, the resting fluorescence, which corresponds to nominally 0 Ca^{2+}, is significantly higher than with dyes that increase their fluorescence with Ca^{2+}. Second, the achievable imaging contrast is high because healthy cells are characterized by very low resting Ca^{2+}, and the dye in adjacent structures, exposed to millimolar Ca^{2+} concentrations, is essentially not fluorescent. Third, since the dynamic range of the fluorescence is ~1 after subtraction of fluorescence at saturating Ca^{2+}, these measurements allow a better quantitative estimation of the Ca^{2+} signals. An example of V_m and Ca^{2+} optical signals recorded sequentially from the two indicators in three different regions on the dendritic tree of a Purkinje neuron stained by JPW-1114 and Fura-FF is illustrated in Fig. 4.3. Using an excitation band of 387±5 nm for Fura-FF (Fig. 4.3a), the Ca^{2+} increase associated with a climbing fibre excitatory postsynaptic potential (EPSP) corresponds to a negative $\Delta F/F_0$ (Fig. 4.3b). Sequential V_m and Ca^{2+} recording using Fura Ca^{2+} indicators has been done in CA1 hippocampal pyramidal neurons (Canepari et al. 2007), in prefrontal cortex layer-5 pyramidal neurons (Milojkovic et al. 2007) and in cerebellar Purkinje neurons (Canepari and Vogt 2008). Sequential recording (as well as signal averaging) is meaningful only if repeated application of the same stimulation protocol results in the same response. This requirement must be confirmed experimentally by comparing individual recordings as shown in Fig. 4.3c. In this example, the V_m and the Ca^{2+} optical signals were recorded from a dendritic location on a cerebellar Purkinje neuron in response to four repetitions of climbing fibre activation separated by 1 minute. The results showed that signals were practically identical in 4 individual trials (gray traces) permitting the correlation of V_m and Ca^{2+} optical signals recorded sequentially in response to the same stimulus.

An important aspect of combined V_m and Ca^{2+} imaging is the interpretation of Ca^{2+} optical signals, which depends on how much the Ca^{2+} indicator perturbs the physiological Ca^{2+} homeostasis. The buffering capacity of a Ca^{2+} indicator, K_{dye}, defined as the ratio between the dye-bound Ca^{2+} and the

free Ca^{2+} in the presence of the indicator depends on the dissociation constant and on the concentration of the indicator (Table 4.1). The perturbation of the physiological Ca^{2+} introduced by the Ca^{2+} indicator can be evaluated by comparing the parameter K_{dye} with the endogenous buffering capacity of the cell (K_{cell}). The interpretation of Ca^{2+} optical signals is simplified when K_{dye} is either much larger or much smaller than K_{cell}, i.e. when most of Ca^{2+} binds to the indicator or when the fraction of Ca^{2+} bound to the indicator is negligible compared to the total Ca^{2+} (Canepari et al. 2008). Without addressing in detail the issue of calibration of Ca^{2+} optical signals (Neher 2000) in this volume focused on V_m imaging, we will note that, in the first case, the $\Delta F/F_0$ signal associated with Ca^{2+} increase is approximately linear with the total intracellular Ca^{2+} signal. In the second case, the time course of the ratio $(F-F_{min})/(F_{max}-F)$, where F_{min} and F_{max} are the fluorescence intensities at 0 and saturating Ca^{2+} respectively, is linear with the physiological intracellular free Ca^{2+} concentration change ($\Delta[Ca^{2+}]_i$). In many instances, Ca^{2+} signals are due to Ca^{2+} influx through a Ca^{2+} channel in the plasma membrane. The contribution to the change in membrane potential due to the Ca^{2+} influx depends on the Ca^{2+} permeability of the channel relative to its permeability to other ions, in particular to Na^+ and K^+. This is different for VGCCs, AMPA receptors, NMDA receptors and other Ca^{2+} permeable pores such as transient receptor potential (TRP) channels. *Vice-versa*, because opening or unblocking of Ca^{2+} channels often depends, in a non-linear manner, on the local membrane potential, the Ca^{2+} influx is often, but not always, larger when the voltage related depolarizing optical signal is larger (Canepari et al. 2007). Because this bi-directional relationship is complex, the analysis of V_m and Ca^{2+} signals from multiple sites on individual neurons is not straightforward and requires careful interpretation.

A notable application of combined V_m and Ca^{2+} imaging is the study of synaptic plasticity where the supra-linear Ca^{2+} signal plays an important role. The supra-linear Ca^{2+} signal occurs when two stimulation protocols are combined to evoke the coincident activity (pairing protocol) which results in a Ca^{2+} signal that is larger than the sum of the two Ca^{2+} signals associated with the application of individual stimulation protocols. A supra-linear Ca^{2+} signal is always caused by a supra-linear $\Delta[Ca^{2+}]_i$, but not necessarily by a supra-linear Ca^{2+} influx through the plasma membrane. Indeed, the supra-linear Ca^{2+} signal might be caused by Ca^{2+} release from internal stores or by the saturation of the endogenous Ca^{2+} buffer. However, in the latter case, if the buffering capacity of the dye dominates over the endogenous buffering capacity of the cell and the dye is not saturated, the presence of the indicator will cancel the supra-linear $\Delta[Ca^{2+}]_i$ and no Ca^{2+} dependent $\Delta F/F_0$ will be observed. Thus, in these conditions, detection of supra-linear Ca^{2+} dependent $\Delta F/F_0$ signals which are not due to Ca^{2+} release from internal stores always corresponds to a supra-linear Ca^{2+} influx and it must always correlate with an increase in the depolarizing V_m signal. In contrast, if the buffering of the dye is negligible compared to the endogenous buffering of the cell, a supra-linear $\Delta[Ca^{2+}]_i$ signal that is due to the saturation of the

endogenous Ca^{2+} buffer can be measured reliably. The two different types of supra-linear Ca^{2+} signals not involving Ca^{2+} release from stores are illustrated by the two following examples.

In measurements from CA1 hippocampal pyramidal neurons (Canepari et al. 2007), cells were loaded with the voltage-sensitive dye JPW-3028 and 300 µM Bis-Fura-2. The purpose of these experiments was to analyze, over large regions of the dendritic tree, the V_m and Ca^{2+} optical signals associated with back-propagating action potentials, with excitatory postsynaptic potentials (EPSPs) and with pairing of these two membrane potential transients using an LTP induction protocol. Pyramidal neurons in the CA1 region are characterized by relatively low endogenous buffering capacity in the dendrites (~100) and even lower buffering capacity (~20) in the spines (Sabatini et al. 2002). Thus, the buffering capacity of 300 µM Bis-Fura-2 (K_d~500 in the presence of Mg^{2+}, see Table 4.1) is ~6 times larger than the buffering capacity of the dendrite and ~30 times larger than the buffering capacity of the spine. Ca^{2+} signals associated either with back-propagating action potentials or with EPSPs were mediated by Ca^{2+} influx through voltage-gated Ca^{2+} channels and/or through NMDA receptors. As shown in Fig. 4.4a, the pairing of the two stimulating protocols elicited a supra-linear Ca^{2+} signal. In the presence of the NMDA receptor blocker AP-5, since the measurements were done using a non-saturating concentration of a high-affinity indicator, the supra-linear Ca^{2+} signal must have been caused by supra-linear Ca^{2+} influx mediated by recruitment of additional VGCCs. In agreement with this expectation, at each site where a supra-linear Ca^{2+} signal was observed, the V_m related optical signal during the pairing protocol had a larger peak depolarization compared to the signals associated with unpaired stimulations (Fig. 4.4a).

In measurements from cerebellar Purkinje neurons (Canepari and Vogt 2008), cells were loaded with 1 mM of the Ca^{2+} indicator Fura-FF and with the voltage sensitive dye JPW-1114. Purkinje neurons have an exceptionally high dendritic K_{cell} estimated at ~2000 (Fierro and Llano 1996). Therefore, the addition of a low affinity Ca^{2+} indicator such as Fura-FF (K_d~10), even at millimolar concentrations, does not significantly alter the physiological homeostasis and it is possible to record changes in free intracellular Ca^{2+} concentration ($\Delta[Ca^{2+}]_i$ signals (Canepari et al. 2008). In this particular preparation, it was possible to calibrate V_m signals in terms of membrane potential. As shown in Fig. 4.4b, pairing the stimulation of the large climbing fibre synaptic potential with local parallel fibres stimulation generated a local dendritic supra-linear $\Delta[Ca^{2+}]_i$ signal which was independent of Ca^{2+} release from stores (Brenowitz and Regehr 2005). Although the $\Delta[Ca^{2+}]_i$ signal originated from Ca^{2+} influx through VGCCs, in Purkinje neurons, in contrast to CA1 pyramidal neurons, the V_m signal during the pairing protocol did not have larger peak depolarization compared to the V_m signals associated with unpaired stimulations (Fig. 4.4b). In this case the Ca^{2+} influx associated with the climbing fibre synaptic potential was the same in paired and unpaired conditions. The corresponding $\Delta[Ca^{2+}]_i$ signal, however, was larger

following paired stimulation because the Ca^{2+} influx associated with the parallel fibre stimulation locally and transiently saturated the endogenous Ca^{2+} buffer (Canepari and Vogt 2008). This supra-linear Ca^{2+} signal could be correctly interpreted only when recorded using a low-affinity indicator. When the cell was injected with 10 mM Bis-Fura-2, K_{dye} became ~10 times larger than K_{cell} and supra-linear Ca^{2+} signals were abolished (Canepari and Vogt 2008).

3.2 Simultaneous V_m and Ca^{2+} imaging

Sequential V_m and Ca^{2+} imaging produce valid results if identical responses are evoked in repetitive measurements. Many physiological processes, however, are stochastic, showing large trial-to-trial variability. In these cases, the study of the time variability contains important biological information and simultaneous V_m and Ca^{2+} optical measurement is required. Simultaneous V_m and Ca^{2+} imaging was initially achieved using the Ca^{2+} indicator Calcium Orange, which has excitation peak at ~550 nm and emission peak at ~580 nm (Sinha et al. 1995; Sinha and Saggau 1999), or with blue-excitable indicators (Bullen et al. 1997; Bullen and Saggau 1998). These possibilities may have, however, some inherent problems. First, the small overlap between the emission spectra of the two dyes may produce a "bleeding" of the V_m signal into the Ca^{2+} recording channel that contaminates the signal. In some situations, such emission cross talk can be mathematically corrected (Sinha, Patel and Saggau 1995). Second, while V_m recordings of synaptic or action potentials can be often achieved within short time, the complete time-course of the corresponding Ca^{2+} signal may require longer acquisition intervals (Canepari, Vogt and Zecevic 2008). In this case, the voltage sensitive dye is exposed to high intensity light for a longer time than what would be required for the V_m measurement alone, increasing both bleaching of the dye and phototoxicity. Simultaneous V_m and Ca^{2+} imaging was also performed using the combination of an absorption voltage sensitive dye with a fluorescent Ca^{2+} indicator. Using bath application of the absorption dye RH-482 and a low-affinity Ca^{2+} indicator Magnesium Green, Sabatini and Regehr could correlate the Ca^{2+} signal underlying synaptic release with the excitation of pre-synaptic terminals in cerebellar synapses (Sabatini and Regehr 1996; Sabatini and Regehr 1997). In these experiments, simultaneous Ca^{2+} and V_m measurements were done by using excitation light wavelength of ~500 nm and recording simultaneously fluorescence from the Ca^{2+} indicator Magnesium Green and the transmitted light from voltage-sensitive dye RH-482 at 710 nm from a single location with two photodiodes. The important limitation of this approach is that the absorption measurements from multiple sites on individual neurons are substantially less sensitive compared to fluorescence measurements (Antic and Zecevic 1995). In the above example, extensive temporal and spatial signal averaging over a large region of the cerebellar slice, which could be obtained with absorption signals, permitted signal detection from presynaptic terminals (Sabatini and Regehr 1997).

The above mentioned problems of simultaneous V_m and Ca^{2+} imaging using the same excitation wavelength can be overcome by using a Fura indicator. The realization of this measurement, however, required the design of a dedicated apparatus (Vogt et al. 2011a) to optimize the signal-to-noise ratio (S/N). In principle, di-8-ANEPPS and JPW-1114 could be excited by blue light in the configuration shown in Fig. 4.1c. However, narrow-band laser excitation at 532 nm or at 543 nm is associated with much larger sensitivity (Canepari et al. 2010) permitting single-trial recordings. These excitation wavelengths are longer than the emission peak of Fura indicators. To allow transmission of V_m and Ca^{2+} emission wavelengths, while reflecting intermediate excitation wavelength (543 nm), the apparatus included a dual-band pass dichroic mirror as shown in the schematic in Fig. 4.5a. Multiple wavelengths dichroic mirrors are commercially available from several companies (e. g. Semrock). The mirror that was used in this case reflected 543 nm and transmitted lower green and red wavelengths corresponding to the emissions of Fura and JPW1114 indicators respectively. This optimal configuration allowed resolving dendritic excitation and associated Ca^{2+} signals from relatively small regions in single trial measurements. In the example shown in Fig. 4.5b, simultaneous ΔV_m and $\Delta[Ca^{2+}]_i$ signals, calibrated as described in Canepari and Vogt (2008), associated with one climbing fibre-EPSP and a train of five parallel fibre EPSPs at 100 Hz were compared in two small dendritic regions. ΔV_m and $\Delta[Ca^{2+}]_i$ signals associated with large depolarization could be observed in both regions for the climbing fibre EPSP but only near the parallel fibre stimulating electrode, for the parallel fibre EPSPs train. These measurements, where signals of ~1% change of fluorescence could be resolved from regions of few microns, represent the current state-of-the-art in sensitivity of simultaneous V_m and Ca^{2+} imaging from single cells.

3.3 Simultaneous optical measurement of V_m and Ca^{2+} currents

Simultaneous V_m and Ca^{2+} imaging can be also used for the study of native fast Ca^{2+} currents based on derivation of Ca-currents from optical signals., We have already stated that the $\Delta F/F_0$ Ca^{2+} signal is proportional to the change in concentration of Ca^{2+} ions bound to the indicator. If, in addition, the Ca^{2+} bound to the indicator is also proportional to the total free Ca^{2+} flux entering the cell through the plasma membrane, then the Ca^{2+} current can be estimated by the derivative of $\Delta F/F_0$ (Sabatini and Regehr 2008). This estimate is possible with low-affinity indicators (Kao and Tsien 1988) where the equilibration of the dye-Ca^{2+} binding reaction is faster than the Ca^{2+} influx. It was recently demonstrated that the reaction between Ca^{2+} and low-affinity indicator Oregon Green 488 BAPTA-5N is faster than a typical VGCC-mediated current, i.e. the $\Delta F/F_0$ signal from this indicator matches the kinetics of the Ca^{2+} current integral (Jaafari et al. 2014). It follows that the kinetics of the $\Delta F/F_0$ derivative is proportional to the kinetics of the Ca^{2+} current and can be calibrated in terms of "Ca^{2+} current volume density". The

simultaneous V_m optical measurement allows studying the voltage dependence of the current, i.e. the membrane potential of activation and inactivation of the channel. Technically, simultaneous V_m and Ca^{2+} imaging using Oregon Green 488 BAPTA-5N requires blue illumination for both indicators (see previous paragraph) and high-speed acquisitions (20 kHz frame rate) to investigate the time-course of the Ca^{2+} current at high temporal resolution. Fig. 4.6a shows an example of a CA1 hippocampal pyramidal neuron filled with 1 mM of Oregon Green 488 BAPTA-5N and the voltage sensitive dye JPW1114. Fig. 4.6b shows the Ca^{2+} current volume density (I_{Ca}/V) associated with an action potential monitored optically in the proximal apical dendritic segment of a CA1 hippocampal pyramidal neuron. The I_{Ca}/V and V_m signals were measured under two conditions: for an action potential starting at V_m = -60 mV and for an action potential starting at V_m = -80 mV (Fig. 4.6b). When the action potential started at V_m = -80 mV, I_{Ca}/V was larger and started at a more hyperpolarized V_m (Fig. 4.6c), indicating that at V_m = -80 mV Ca^{2+} current contained a component mediated by low-voltage activated (T-type) Ca^{2+} channels (Cueni et al. 2009). The example shown in Fig. 4.6 illustrates how simultaneous optical measurement of V_m and Ca^{2+} currents can drastically improve our understanding of the physiological function of Ca^{2+} channels by permitting the exploration of local biophysics of native channels during physiological activity.

4 Combining V_m imaging with photostimulation

4.1 Combining V_m imaging with glutamate or GABA photorelease

Membrane potential imaging can be combined with uncaging techniques to investigate how the photorelease of biologically active molecules changes the membrane potential in different regions of a cell. In particular, the caged compounds 4-Methoxy-7-nitroindolinyl-caged-L-glutamate (MNI-glutamate, Canepari et al. 2001) and 1-(4-Aminobutanoyl)-4-[1,3-*bis*(dihydroxyphosphoryloxy)propan-2-yloxy]-7-nitroindoline (DPNI-GABA, Trigo et al. 2009) can be used to obtain fast photorelease of either L-glutamate or GABA in sub-cellular regions of variable size and to investigate the regulation of membrane potential. An example of this methodological approach is the study of shunting inhibition (Mann et al. 2007). Propagation of action potentials in the axon or back-propagation of action potentials in the dendrites can be strongly regulated by local changes of membrane conductance due to opening of $GABA_A$ receptors. Simultaneous V_m imaging and GABA photorelease is an ideal approach to investigate shunting inhibition. In the CA1 hippocampal pyramidal neuron shown in Fig 4.7a, the effect of local GABA photorelease on the back-propagating action potential in the apical dendrite was

explored. DPNI-GABA was applied using a patch pipette positioned close to the distal part of the dendrite at ~200 µm from the soma. The fluorescence change associated with a back-propagating action potential under control conditions (Fig. 4.7b, left traces) was compared with a back-propagating action potential occurring 15 ms after an episode of GABA photorelease (Fig. 4.7b, right traces) from four regions of interest. The amplitude of the somatic action potential was the same in both cases, but local GABA uncaging decreased the amplitude of the fluorescence change associated with the back-propagating action potential progressively with the distance from the soma. Although shunting inhibition induced by GABA uncaging is produced by non-physiological co-activation of synaptic and extra-synaptic GABA receptors, this experiment represents a useful model of this phenomenon since it permits a clear separation of presynaptic and postsynaptic effects, a clear localization of the activated GABA receptors and the possibility to perform pharmacological studies that cannot be done using presynaptic stimulation. Thus, combining membrane potential imaging with GABA photorelease shows the spatial restriction of the shunting effect and the resulting rapid loss in action potential backpropagation.

4.2 Using glutamate uncaging to calibrate voltage-sensitive dyes signals

The calibration of V_m optical signals on an absolute scale (in mV) provides direct measurements of V_m signal amplitudes from multiple locations. This information can be used to construct and analyze the dynamic spatial maps of signal amplitudes throughout neuronal processes. The temporally and spatially well resolved maps of activity are one of the key elements in understanding the rules governing dendritic signal processing and plasticity. The absolute calibration of optical V_m signals, however, is not straightforward and often the exact callibration is not possible. Voltage-sensitive dye recording of membrane potential transients belongs to a class of indirect measurements. The quantity that is being measured directly, by photodetectors, is light intensity, and the quantity that needs to be monitored is derived from a known relationship between the light intensity and V_m. It is convenient that the relationship between light intensity and V_m is strictly linear over the entire physiological range for many voltage sensitive dyes (e. g. Gupta et al. 1981; Loew and Simpson 1981; Wu and Cohen 1993). In a multisite recording, the fractional change in light intensity is proportional to V_m, but also, to a different extent at different sites, to an additional factor: the ratio of inactive dye to active dye. The inactive dye is bound to connective tissue or any other membranes that do not change potential while the active dye is bound to the excitable membrane being monitored. The inactive dye contributes to the resting fluorescence only, and the light from active dye contributes to the resting fluorescence and also carries the signal. In experiments utilizing intracellular application of the dye, inactive dye would be bound to intracellular membranes and organelles. It is a general rule that the ratio of active dye to inactive dye is different for different regions of the object and is also unknown. It follows that the sensitivity of recording

from different regions of the object will be different and the calibration of all detectors cannot be done by calibrating the optical signal from any single site. In this situation, the calibration is absolute and straightforward if a calibrating electrical signal that has known amplitude at all locations is available. An all-or-none action potential signal is ideal for this purpose and can be used to create a sensitivity profile of the measuring system. This type of calibration was used to scale the amplitudes of sub-threshold signals in mitral cells of the olfactory bulb (Djurisic et al. 2004). If action potentials are not available, another type of calibrating electrical signal can be a slow electrical change spreading with minimal attenuation over relatively long distances. Such condition occurs, for instance, in cerebellar Purkinje neurons (Roth and Hausser 2001; Canepari et al. 2008).

The possibility to achieve uniform depolarization over the entire dendritic tree using L-glutamate photolysis may extend the possibility to calibrate fluorescence signals to other cell types. This calibration procedure is based on the principle that if the ionotropic glutamate receptor becomes the dominant conductance in a particular neuronal compartment, its reversal potential will determine the membrane potential of the compartment. Thus, if dominance of glutamate receptor conductance is obtained by L-glutamate uncaging, the resulting V_m change in different compartments of the neuron will be the same and can be used to calibrate voltage-sensitive dye imaging data. The idea of a calibration protocol based on L-glutamate uncaging relies on saturating depolarization in the visualized area (Vogt et al. 2011b). The fractional change of fluorescence will then correspond to the resting membrane potential in each visualized site where photolysis occurs.

In the CA1 hippocampal pyramidal neuron of Fig. 4.8a, one action potential was evoked by somatic current injection. The fractional changes of fluorescence associated with the back-propagating AP from four ROIs on the apical dendrites are shown in Fig. 4.8b (left traces). The amplitude of the signal is variable and could not be directly correlated with the absolute change of membrane potential. After addition of 1 µM TTX, to block action potentials, and of 50 µM CTZ, to prolong depolarization by blocking AMPA receptor desensitization, L-glutamate was photoreleased over the whole field of view. The recording was performed starting from the resting V_m of the cell. The size of the fluorescence change at each site and the absolute somatic depolarization elicited by uncaging increased with the amount of released L-glutamate, i.e. with the exposure time of the UV light, eventually reaching saturation. The saturating V_m corresponded to the reversal potential of glutamate receptors. Using this information, the amplitude of the back-propagating action potential signals was converted into the change in membrane potential. This method of calibration of voltage-sensitive dyes signals, based on L-glutamate photorelease, can only be applied to cell types characterized by dominant glutamate conductance.

4.3 Combining V_m imaging with ChR stimulation

For control of neuronal activity, optogenetic approaches based on light-sensitive channels and other photo-reactive molecules enable highly selective control of genetically-defined populations of neurons (Mancuso et al. 2011; Yizhar et al. 2011). Such techniques offer high time resolution and high spatial precision, allowing stimulation of either individual neurons or large neuronal populations. A commonly used protein for this application is Channelrhodopsin2 (ChR2, Zhang et al. 2006). Combination of optical stimulation using ChR2, with membrane potential imaging is in principle a potent approach to investigate electrical activity both at cellular and at network level. The accomplishment of this type of experiment, however, requires voltage-sensitive dyes that are excitable by red wavelengths since activation of ChR2 occurs at visible wavelengths <600 nm. Indicators with these characteristics have been developed by Rina Hildensheim and Amiram Grinvald to investigate electrical activity from the entire cortex *in vivo* without optical interference of hemoglobin absorption (Grinvald and Hildensheim 2004). More recently, red or near-IR excitable or fluorescent indicators have been developed by Joseph Wuskell, Ping Yan and Leslie Loew to monitor electrical activity in the heart (Matiukas et al. 2005) and in the brain (Wuskell et al. 2006) or to be injected in individual cells (Zhou et al. 2007; Yan et al. 2012). Among these new voltage sensitive dyes, five have been specifically tested to be used in combination with ChR2 stimulation (Kee et al. 2008). In the example shown in Fig. 4.9a (modified from Tsuda et al. 2013), ChR2 was selectively expressed in interneurons located in the molecular layer, providing inhibitory post-synaptic potentials (IPSPs) to cerebellar Purkinje neurons when the light-sensitive channel was excited. In this experiment, the cerebellar slice was stained with the voltage sensitive dye Di-2-ANBDQPQ (Zhou et al. 2007) and excited at 658 nm, beyond the excitation spectrum of ChR2 (Kee et al. 2008). Transient photo-stimulation of the molecular layer with blue light produced an IPSP in the nearby Purkinje neurons. As shown in Fig. 4.9a, the IPSP elicited by photo-stimulation of the molecular layer could be measured optically. Notably, the kinetics of the optical signal was identical to that of the IPSP measured with a patch electrode. In another study, ChR2 was selectively expressed in GABAergic interneurons of the hippocampal *stratum lacunosum moleculare* and the regulation of electrical activity in different areas was characterized by staining the slice with the indicator DI-4-ANBDQPQ (Kee et al. 2008) and by performing V_m imaging (Leão et al. 2012). Thus, using this strategy, it was possible to determine that interneurons from the stratum lacunosum molecular differentially modulate CA3 and entorhinal inputs to hippocampal CA1 neurons.

Using water soluble indicators excitable with red light (Zhou et al. 2007; Yan et al. 2012), electrical activity can be imaged in combination with ChR2 photostimulation from individually stained cells (Willadt et al. 2014). The clear advantage of this approach is that the higher sensitivity of V_m imaging in individually stained neurons permits optical measurements of smaller membrane potential changes from

well identified sub-cellular compartments. In the examples shown in Fig. 4.9b, ChR2 was expressed by all GABAergic interneurons and individual hippocampal cells were filled with the indicator Di-2-ANBDQPTEA. When electrical and optical recordings were performed from a GABAergic interneuron, ChR2 photo-stimulation of the recorded cell generated an action potential that could be monitored both electrically and optically from proximal dendritic segment (Fig. 4.9b, left). In contrast, when electrical and optical recordings were performed from a CA1 pyramidal neuron, ChR2 photo-stimulation of pre-synaptic interneurons generated an IPSP that was recorded both electrically and optically from the proximal part of the apical dendrite (Fig. 4.9b, right). In conclusion, these initial studies indicate that combining membrane potential imaging with optogenetic photostimulation is likely to become a standard approach in the near future.

REFERENCES

Antic S, Zecevic D (1995) Optical signals from neurons with internally applied voltage-sensitive dyes. J Neurosci 15:1392-1405.

Berger T, Borgdorff A, Crochet S, Neubauer FB, Lefort S, Fauvet B, Ferezou I, Carleton A, Lüscher HR, Petersen CC (2007) Combined voltage and calcium epifluorescence imaging in vitro and in vivo reveals subthreshold and suprathreshold dynamics of mouse barrel cortex. J Neurophysiol 97:3751-3762.

Brenowitz SD, Regehr WG (2005) Associative short-term synaptic plasticity mediated by endocannabinoids. Neuron 45:419-431.

Bullen A, Patel SS, Saggau P (1997) High-speed, random-access fluorescence microscopy: I. High-resolution optical recording with voltage-sensitive dyes and ion indicators. Biophys J 73:477-491.

Bullen A, Saggau P (1998) Indicators and optical configuration for simultaneous high-resolution recording of membrane potential and intracellular calcium using laser scanning microscopy. Pflügers Arch 436:788–796.

Bullen A, Saggau P (1999) High-speed, random-access fluorescence microscopy: II. Fast quantitative measurements with voltage-sensitive dyes. Biophys J 76:2272-2287.

Canepari M, Djurisic M, Zecevic D (2007) Dendritic signals from rat hippocampal CA1 pyramidal neurons during coincident pre- and post-synaptic activity: a combined voltage- and calcium imaging study. J Physiol 580:463-484.

Canepari M, Nelson L, Papageorgiou G, Corrie JE, Ogden D (2001) Photochemical and pharmacological evaluation of 7-nitroindolinyl-and 4-methoxy-7-nitroindolinyl-amino acids as novel, fast caged neurotransmitters. J Neurosci Meth 112: 29-42.

Canepari M, Vogt KE (2008) Dendritic Spike Saturation of Endogenous Calcium Buffer and Induction of Postsynaptic Cerebellar LTP. PLoS ONE 3:e4011.

Canepari M, Vogt K, Zecevic D (2008) Combining voltage and calcium imaging from neuronal dendrites. Cell Mol Neurobiol 58:1079-1093.

Canepari M, Willadt S, Zecevic D, Vogt KE (2010) Imaging Inhibitory Synaptic Potentials Using Voltage Sensitive Dyes. Biophys J 98: 2032-2040.

Cueni L, Canepari M, Adelman JP, Lüthi A (2009) Ca2+ signaling by T-type Ca2+ channels in neurons. Pflugers Arch 457:1161–1172.

Djurisic M, Antic S, Chen WR, Zecevic D (2004) Voltage imaging from dendrites of mitral cells: EPSP attenuation and spike trigger zones. J Neurosci 24:6703-6714.

Eilers J, Konnerth A (2000) Dye Loading with Patch Pipettes. In: Yuste R, Lanni F, Konnerth A (ed) Imaging Neurons A Laboratory Manual, Cold Spring Harbour Laboratory Press, New York.

Fierro L, Llano I (1996) High endogenous calcium buffering in Purkinje cells from rat cerebellar slices. J Physiol 496:617-625.

Fluhler E, Burnham VG, Loew LM (1985) Spectra, membrane binding, and potentiometric responses of new charge shift probes. Biochemistry 24:5749-5755.

Gupta RK, Salzberg BM, Grinvald A, Cohen LB, Kamino K, Lesher S, Boyle MB, Waggoner AS, Wang CH (1981) Improvements in optical methods for measuring rapid changes in membrane potential. J Memb Biol 58: 123-137.

Hyrc KL, Bownik JM, Goldberg MP (2000). Ionic selectivity of low-affinity ratiometric calcium indicators: mag-Fura-2, Fura-2FF and BTC. Cell Calcium 27:75-86.

Jaafari N, De Waard M, Canepari M (2014). Imaging Fast Calcium Currents beyond the Limitations of Electrode Techniques. Biophys J 107:1280-1288.

Kao JP, Tsien RY (1988) Ca2+ binding kinetics of fura-2 and azo-1 from temperature-jump relaxation measurements. Biophys J 53:635-639.

Kee MZ, Wuskell JP, Loew LM, Augustine GJ, Sekino Y (2008) Imaging activity of neuronal populations with new long-wavelength voltage-sensitive dyes. Brain Cell Biol 36: 157-172.

Kremer S G, Zeng W, Skorecki K L (1992) Simultaneous fluorescence measurement of calcium and membrane potential responses to endothelin. Am J Physiol 263:1302-1309.

Leão RN, Mikulovic S, Leão KE, Munguba H, Gezelius H, Enjin A, Patra K, Eriksson A, Loew LM, Tort (2012) OLM interneurons differentially modulate CA3 and entorhinal inputs to hippocampal CA1 neurons. Nat Neurosci 15:1524-1530.

Loew LM, Simpson LL (1981) Charge-shift probes of membrane potential: a probable electrochromic mechanism for p-aminostyrylpyridinium probes on a hemispherical lipid bilayer. Biophys J 34:353-365.

Mancuso JJ, Kim J, Lee S, Tsuda S, Chow NB, Augustine GJ (2011) Optogenetic probing of functional brain circuitry. Exp Physiol 96: 26–33.

Mann EO, Paulsen O (2007) Role of GABAergic inhibition in hippocampal network oscillations. Trends Neurosci 30: 343-349.

Martinez-Zaguilan R, Martinez GM, Lattanzio F, Gillies RJ (1991) Simultaneous measurement of intracellular pH and Ca2+ using the fluorescence of SNARF-1 and fura-2. Am J Physiol 260:297-307.

Matiukas A, Mitrea BG, Pertsov AM, Wuskell JP, Wei MD, Watras J, Millard AC, Loew LM (2005) New near-infrared optical probes of cardiac electrical activity. Am J Physiol Heart Circ Physiol 290: H2633-2643.

Milojkovic BA, Zhou WL, Antic SD (2007) Voltage and calcium transients in basal dendrites of the rat prefrontal cortex. J Physiol 585:447-468.

Naraghi M (1997) T-jump study of calcium binding kinetics of calcium chelators. Cell Calcium 22:255-268.

Neher E (2000) Some quantitative aspects of calcium fluorimetry. In: Yuste R, Lanni F, Konnerth A (ed) Imaging Neurons A Laboratory Manual, Cold Spring Harbour Laboratory Press, New York.

Roth A, Häusser M (2001) Compartmental models of rat cerebellar Purkinje cells based on simultaneous somatic and dendritic patch-clamp recordings. J Physiol 535:445-472.

Sabatini BS, Oertner TG, Svoboda K (2002) The life cycle of Ca^{2+} ions in dendritic spines. Neuron 33:439–452.

Sabatini BL, Regehr WG (1996) Timing of neurotransmission at fast synapses in the mammalian brain. Nature 384:170-172.

Sabatini BL, Regehr WG (1997) Control of Neurotransmitter Release by Presynaptic Waveform at the Granule Cell to Purkinje Cell Synapse. J Neurosci 17:3425–3435.

Sabatini BL, Regehr WG (1998) Optical measurement of presynaptic calcium currents. Biophys J 74:1549-1563.

Schneggenburger R, Meyer AC, Neher E (1999) Released fraction and total size of a pool of immediately available transmitter quanta at a calyx synapse. Neuron 23:399-409.

Sinha SR, Patel SS, Saggau P (1995) Simultaneous optical recording of evoked and spontaneous transients of membrane potential and intracellular calcium concentration with high spatio-temporal resolution. J Neurosci Meth 60:49-46.

Sinha SR, Saggau P (1999) Simultaneous optical recording of membrane potential and intracellular calcium from brain slices. Methods 18:204-214.

Trigo FF, Papageorgiou G, Corrie JE, Ogden D (2009) Laser photolysis of DPNI-GABA, a tool for investigating the properties and distribution of GABA receptors and for silencing neurons in situ. J Neurosci Meth 181: 159-169.

Tsuda S, Kee MZ, Cunha C, Kim J, Yan P, Loew LM, Augustine GJ (2013) Probing the function of neuronal populations: combining micromirror-based optogenetic photostimulation with voltage-sensitive dye imaging. Neurosci Res 75:76-81.

Vogt KE, Gerharz S, Graham J, Canepari M (2011a) High-resolution simultaneous voltage and Ca^{2+} imaging. J Physiol 589: 489-494.

Vogt KE, Gerharz S, Graham J, Canepari M (2011b) Combining membrane potential imaging with L-glutamate or GABA photorelease. PLoS ONE 6: e24911.

Willadt S, Canepari M, Yan P, Loew LM, Vogt KE (2014) Combined Optogenetics and Voltage Sensitive Dye Imaging at Single Cell Resolution. Front Cell Neurosci

Wu JY, Cohen LB (1993) Fast multisite optical measurement of membrane potential. In: (Mason WT, ed) Biological Techniques: Fluorescent and Luminescent Probes for Biological Activity, Academic Press, New York.

Wuskell JP, Boudreau D, Wei MD, Jin L, Engl R, Chebolu R, Bullen A, Hoffacker KD, Kerimo J, Cohen LB, Zochowski MR, Loew LM (2006) Synthesis, spectra, delivery and potentiometric responses of new styryl dyes with extended spectral ranges. J Neurosci Methods 151: 200-215.

Yan P, Acker CD, Zhou WL, Lee P, Bollensdorff C, Negrean A, Lotti J, Sacconi L, Antic SD, Kohl P, Mansvelder HD, Pavone FS, Loew LM (2012) Palette of fluorinated voltage-sensitive hemicyanine dyes. Proc Natl Acad Sci U S A 109: 20443-20448.

Yizhar O, Fenno LE, Davidson TJ, Mogri M, Deisseroth K (2011) Optogenetics in neural systems. Neuron 71: 9–34.

Yuste R (2000) Loading Brain Slices with AM Esters of Calcium Indicators. In: Yuste R, Lanni F, Konnerth A (ed) Imaging Neurons A Laboratory Manual, Cold Spring Harbour Laboratory Press, New York.

Zhang F, Wang LP, Boyden ES, Deisseroth K (2006) Channelrhodopsin-2 and optical control of excitable cells. Nat Methods 3: 785-792.

Zhou W-L, Yan P, Wuskell JP, Loew LM, Antic SD (2007) Intracellular long-wavelength voltage-sensitive dyes for studying the dynamics of action potentials in axons and thin dendrites. J Neurosci Meth 164:225–239.

Figure Legends

Figure 4.1. Alternatives for combined imaging using two-indicators. **a)** (Left) Ideal absorption and emission spectra of two indicators with separate absorption spectra and overlapping emission spectra. Arrows indicated by “ex” and “em” are positioned over ideal excitation and emission. Rectangles indicated by “d” are in position of ideal dichroic mirrors. (Right) Optical arrangements for excitation and recording of fluorescence using either one or two light sources. **b)** (Left) Same as a) but for two indicators with overlapping absorption spectra and separate emission spectra. (Right) Optical arrangements for excitation and recording of fluorescence using either one or two light detection systems. **c)** (Left) Same as a) and b) but for two indicators with separate absorption and emission spectra. (Right) Optical arrangements for excitation and recording of fluorescence using either one or two light sources and light detection systems.

Figure 4.2. Absorption and emission spectra of di-8 ANEPPS in combination with the ideal absorption and emission of Calcium Green and Fura calcium indicators. Left and right curves are the absorption and emission spectra as reported by Invitrogen – Molecular Probes. The thick downward arrow represents the excitation of the ratiometric indicator Fura. The thin downward arrows represent the excitation peak of Calcium Green. The upward arrows represent the emission peaks of the two indicators.

Figure 4.3. Combining V_m and Ca^{2+} imaging using JPW-1114 and a UV excitable Ca^{2+} indicator. **a)** Schematic of the imaging apparatus for sequential V_m and Ca^{2+} imaging using a Fura indicator. Filters for voltage-sensitive dye (JPW): ex1 = 525±25 nm, d1 > 570 nm and em1 > 610 nm. Filters for Ca^{2+} indicator (Fura): ex2 = 387±6 nm, d1 > 470 nm and em1 = 510±42 nm. **b)** V_m and Ca^{2+} fractional changes of fluorescence from cerebellar Purkinje neuron dendrites related to a climbing fibre EPSP recorded from the locations 1-3 reported in the fluorescence images on the left. Somatic recording of the climbing fibre EPSP is the upper trace. **c)** Individual V_m (left) and Ca^{2+} (right) fractional changes of fluorescence (gray traces) related to a climbing fibre EPSP. Superimposed black traces are the averages of the four trials.

Figure 4.4. Combining V_m and Ca^{2+} imaging using high- and low-affinity Fura indicators. **a)** (Left) Ca^{2+} and V_m fractional changes of fluorescence corresponding to back-propagating action potentials (bAPs) and paired EPSP–bAP signals from two locations on the dendritic tree of a CA1 hippocampal pyramidal

neuron. Signals are superimposed to reveal the region-specific increase in peak depolarization during paired activity. (Right) Fluorescence image of the dendritic arbor of three hippocampal pyramidal neurons. The stimulating electrode is indicated schematically. (Middle and bottom panels) Color-coded spatial maps of the Ca^{2+} signal and of the V_m signal during paired activity respectively; signals were scaled using the signals in unpaired conditions. Experiments are in the presence of the NMDA receptor blocker AP-5. Supra-linear Ca^{2+} correlated with larger depolarization. Reproduced from Canepari et al. 2007 with the permission of Wiley-Blackwell. **b)** (Top) Recorded dendrites of a cerebellar Purkinje neuron; supra-linear $\Delta[Ca^{2+}]_i$ from the difference between $\Delta[Ca^{2+}]_i$ associated with the pairing protocol and $\Delta[Ca^{2+}]_i$ associated with the unpaired PF-EPSPs and CF-EPSP in color-coded scale. (Bottom) $\Delta[Ca^{2+}]_i$ and ΔV_m from the region square region depicted above associated with 1 unpaired (black traces) and 1 paired CF-EPSP. Supra-linear Ca^{2+} is not associated with larger depolarization. Modified from Canepari and Vogt 2008.

Figure 4.5. Simultaneous V_m and Ca^{2+} imaging. **a)** Schematic of the optical configuration to achieve simultaneous V_m and Ca^{2+} imaging; 543 nm and 387 nm are used for voltage sensitive dye and Fura indicator excitations respectively; low green and red emissions of the two indicators are separated and detected with two cameras. **b)** (Top) Reconstruction of a cerebellar Purkinje neuron with the dendritic area in recording position outlined; two sites of interest (*1* and *2*) are indicated by the arrows. (Bottom) ΔV_m (red traces) and $\Delta[Ca^{2+}]_i$ (blue traces) signals associated with a climbing EPSP (left) or with a train of five parallel fibre EPSPs at 100 Hz (right) from the two sites of interest; somatic electrical recordings shown below. Modified from Vogt et al. 2011a.

Figure 4.6. Dendritic Ca^{2+} currents associated with an action potential at different starting V_m. **a)** Fluorescence images of a CA1 hippocampal pyramidal neuron filled with Oregon Green 488 BAPTA-5N (left image) and the voltage sensitive dye JPW1114 (right image); the region of interest from where fluorescence was averaged is outlined. **b)** Ca^{2+} currents (blue) associated with one action potential starting either at V_m = -60 mV or -80 mV; V_m recorded optically (red) and with the electrode (black) superimposed. **c)** Ca^{2+} currents normalized and superimposed to the action potential in the two cases; V_m at the current onset (V_m^0) indicated. Modified from Jaafari et al. 2014.

Figure 4.7. Investigating shunting inhibition using combined V_m imaging and local GABA photorelease. **a)** Image of a CA1 hippocampal pyramidal neuron; the dendritic area in recording position is outlined and four regions of interest are shown on the right; the position of the pipette used for caged-glutamate application is illustrated. **b)** V_m optical signals from the regions *1-4* and somatic recordings associated

with one back-propagating action potential elicited by somatic current injection in control condition (left) and 15 ms after an episode of 1 ms GABA photorelease (right). The optical signals are normalized to the peaks of the spike in control condition; the length of the double-arrow corresponds to the peak. Modified from Vogt et al. 2011b.

Figure 4.8. Calibration of fractional changes of fluorescence in terms of membrane potential using L-glutamate **a)** Image of a CA1 hippocampal pyramidal neuron; the dendritic area in recording position is outlined and four regions of interest are shown on the right; caged-glutamate is applied over the visualized area of the dendrite and wide-field illumination was used for photolysis. **b)** (Left) V_m optical signals from the regions of interest *1-4* and somatic recordings associated with one back-propagating action potential. (Right) After addition of 1 µM TTX and 50 µM CTZ, V_m optical signals from the same regions and somatic recordings associated with 1 ms L-glutamate photo-release. The peaks of the somatic signal are indicated over their respective traces; the sizes of the estimated peak spikes in the regions of interest are indicated over their respective traces. Modified from Vogt et al. 2011b.

Figure 4.9. Combining V_m imaging with ChR2 stimulation. **a)** (Left) Schematic of the optical configuration to achieve this combination; red and blue illumination are used for voltage sensitive dye and ChR2 excitations respectively; IR fluorescence emission is detected. (Right) IPSP recorded electrically (with a patch electrode) and optically from a the soma of a Purkinje neuron following ChR2 excitation at interneurons located in the molecular layer; modified from Tsuda et al. 2013 **b)** Imaging of light evoked action potential in a ChR2 expressing interneuron (left) and of IPSP in CA1 pyramidal neuron induced by ChR stimulation at interneurons (right). (Top) Schematic illustrations of the experiment on the top with site of blue flash and imaging region. (Bottom) Simultaneous optical dendritic and electrical somatic recordings; arrows indicate blue light application (5 ms); modified from Willadt et al. 2014.

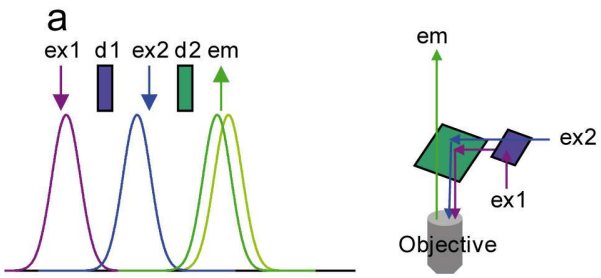
a
ex1 d1 ex2 d2 em
em
ex2
ex1
Objective

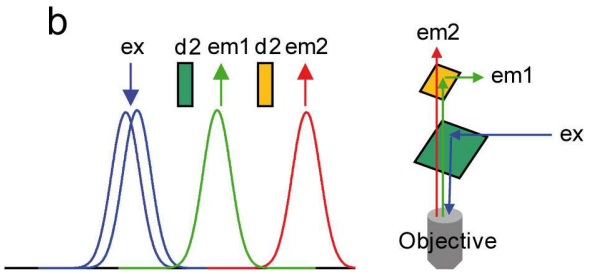
b
ex d2 em1 d2 em2
em2
em1
ex
Objective

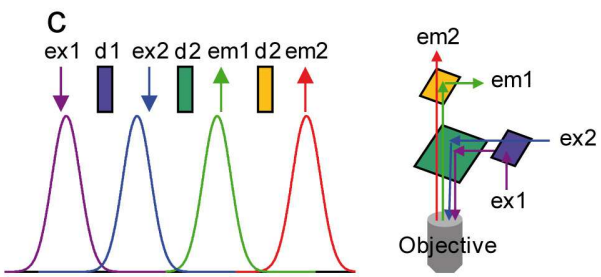
c
ex1 d1 ex2 d2 em1 d2 em2
em2
em1
ex2
ex1
Objective

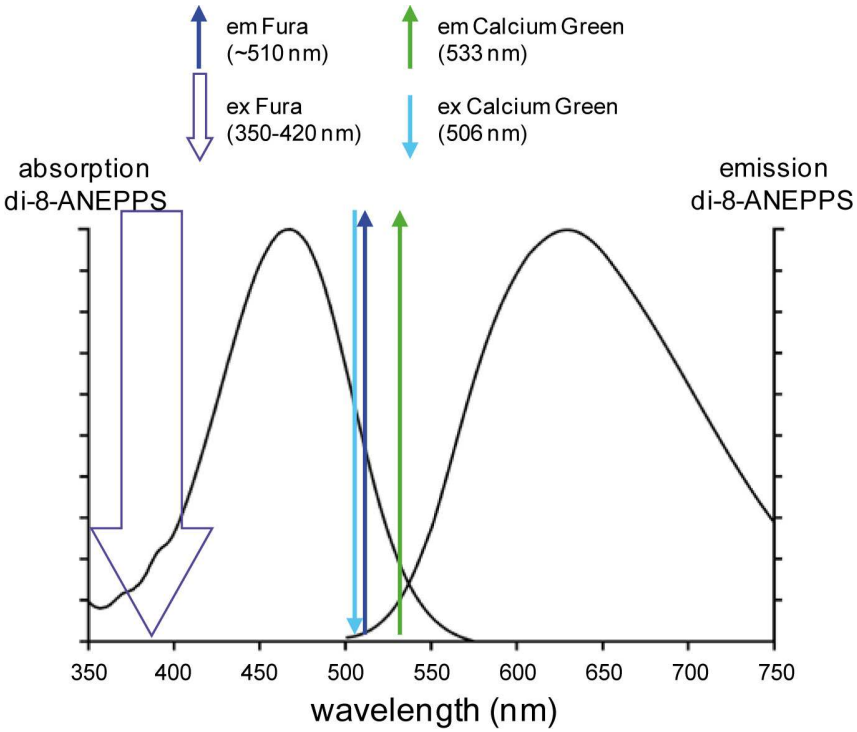
em Fura
(~510 nm)
em Calcium Green
(533 nm)
ex Fura
(350-420 nm)
ex Calcium Green
(506 nm)
absorption
di-8-ANEPPS
emission
di-8-ANEPPS
350 400 450 500 550 600 650 700 750
wavelength (nm)

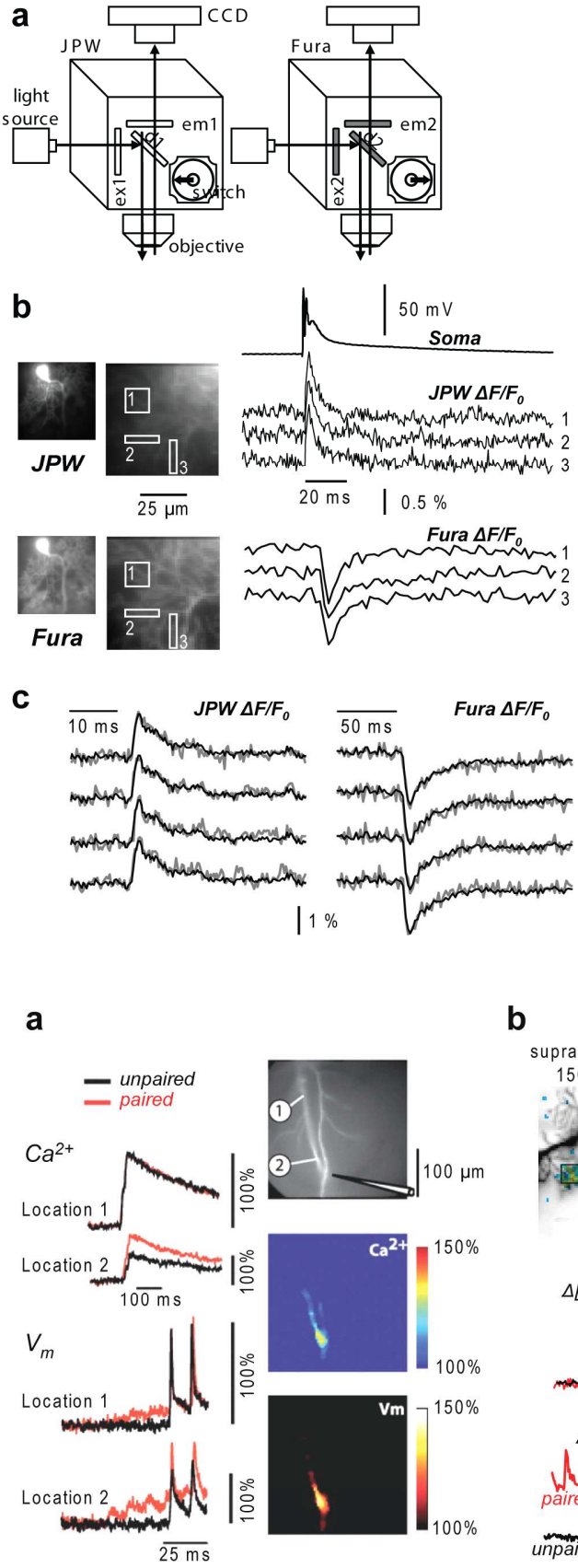
a
CCD
JPW
Fura
light source
em1
em2
ex1
ex2
switch
objective
b
50 mV
Soma
JPW ΔF/F0
1
2
3
JPW
25 µm
20 ms
0.5 %
Fura ΔF/F0
Fura
c
10 ms
JPW ΔF/F0
50 ms
Fura ΔF/F0
1 %
a
unpaired
paired
Ca2+
Location 1
Location 2
100 ms
100%
100 µm
150%
Vm
25 ms
b
supra-linear Ca2+(nM)
150
300
50 µm
stim
Δ[Ca2+]i
0.25 µM
100 ms
ΔVm
20 mV
25 ms

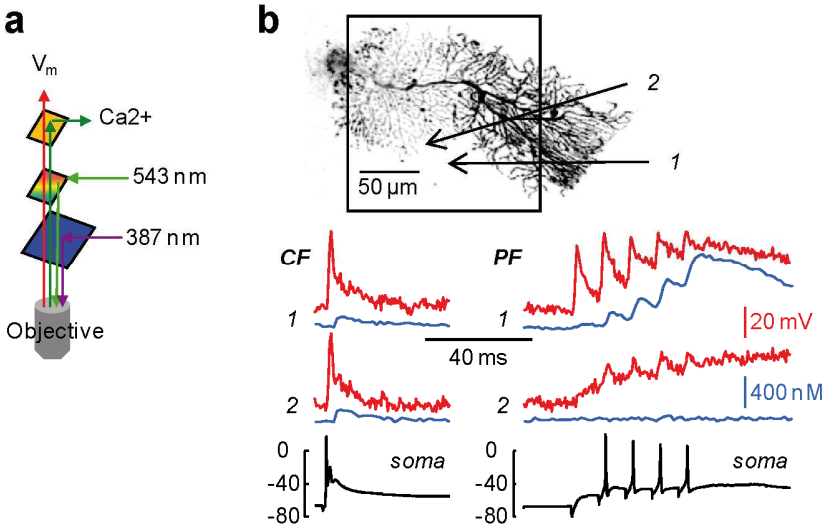
a
Vm
Ca2+
543 nm
387 nm
Objective
b
2
1
50 µm
CF
PF
1
1
20 mV
40 ms
2
2
400 nM
0
-40
-80
soma
0
-40
-80
soma

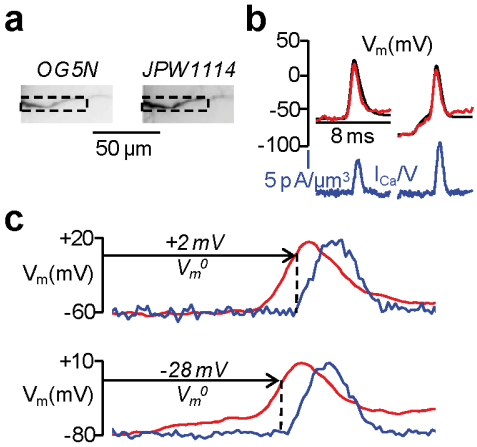
a
OG5N
JPW1114
50 µm
b
50
0
-50
-100
Vm(mV)
8 ms
5 pA/µm3
ICa/V
c
+20
Vm(mV)
-60
+2 mV
Vm0
+10
Vm(mV)
-80
-28 mV
Vm0

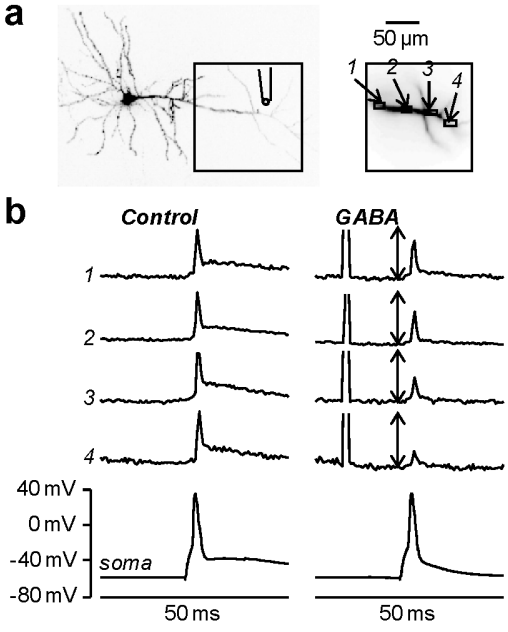
a
50 µm
1
2
3
4
b
Control
GABA
1
2
3
4
40 mV
0 mV
-40 mV
-80 mV
soma
50 ms
50 ms

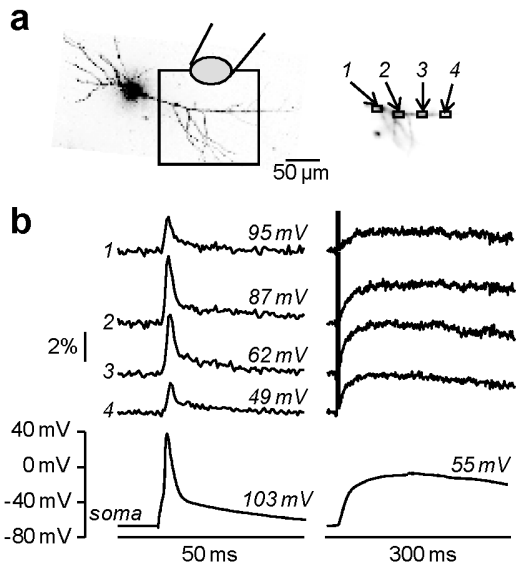
a
1 2 3 4
50 µm
b
95 mV
87 mV
62 mV
49 mV
2%
40 mV
0 mV
-40 mV
-80 mV
soma
103 mV
55 mV
50 ms
300 ms

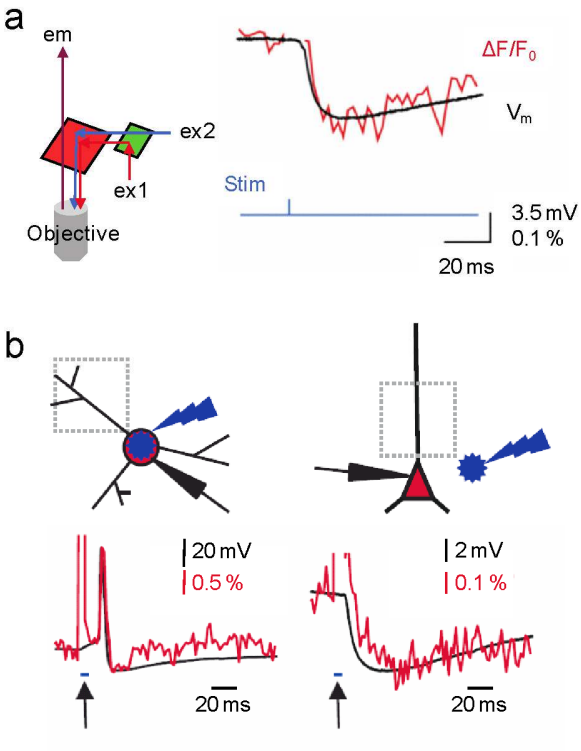
a
em
ex2
ex1
Objective
ΔF/F0
Vm
Stim
3.5 mV
0.1 %
20 ms
b
20 mV
0.5 %
20 ms
2 mV
0.1 %
20 ms